Available online at www.sciencedirect.com
SCIENCE DIRECT®
Journal of Photochemistry and Photobiology A: Chemistry 167 (2004) 201–212
Journal of Photochemistry and Photobiology A:Chemistry
www.elsevier.com/locate/jphotochem

Electronic excitation spectra and singlet–triplet coupling in psoralen and its sulfur and selenium analogs

Jörg Tatchen, Martin Kleinschmidt, Christel M. Marian*

Institute of Theoretical and Computational Chemistry, Heinrich-Heine-Universität, Universitätsstr. 1, D-40225 Dusseldorf, Germany

Received 23 April 2004; accepted 25 May 2004

Available online 23 July 2004

Abstract

We have calculated the vertical singlet and triplet excitation spectra and spin–orbit coupling matrix elements for psoralen and its derivatives resulting from the replacement of intracyclic oxygen by sulfur or selenium. Molecular ground state equilibrium geometries have been determined employing Kohn–Sham density functional theory. Electronic excitation energies and oscillatory strengths have been obtained utilizing a combined density functional/multi-reference configuration interaction method. Spin–orbit coupling matrix elements for correlated wavefunctions have been computed applying the efficient, purely non-empirical spin–orbit mean-field approximation.

The theoretical data allows for a detailed assignment of experimental absorption bands [J. Photochem. Photobiol. B: Biol. 35 (1996) 221]. The computed excitation energy of the first $\pi \rightarrow \pi^*$ singlet transition varies from 3.81 (7H-furo [3,2-g] [1] benzopyran-7-one) to 3.12 eV (7H-selenolo [3,2-g] [1] benzoselenopyran-7-one). The energy of the lowest triplet $\pi \rightarrow \pi^*$ state T_1 is remarkably constant in all cases (2.95–2.73 eV). The energies of the dark $n \rightarrow \pi^*$ states are found to be lowered considerably (up to ≈0.80 eV) upon replacing intracyclic oxygen at the pyrone side by sulfur or selenium, but much less upon hetero-atom substitution solely at the furan side. For all the heteropsoralens, additional low-lying $\pi \rightarrow \sigma^*$ states have been found that are important for photochemical ring opening reactions.

The spin–orbit coupling between the T_1 state and the ground state S_0 amounts to less than $2\,cm^{-1}$ for all cases. Between $n \rightarrow \pi^*$ and $\pi \rightarrow \pi^*$ states appreciable spin–orbit coupling matrix elements are observed which indicate a probable channel for singlet–triplet radiationless transitions. Their size varies from several ten wavenumbers for those psoralens which have oxygen or sulfur in the pyrone ring to several hundred wavenumbers in the case when selenium is present in the pyrone ring.

Keywords: Spin–orbit coupling; Multi-reference configuration interaction; Excited states; Psoralen; Photodynamic therapy

1. Introduction

Psoralens (also called furocoumarins) are a class of photobiologically active substances which are of pharmaceutical use in many respects [1,2]. In a PUVA therapy (psoralen plus ultraviolet A or UV-A radiation) of skin diseases, oral or topical application of psoralens is combined with the exposure of the diseased skin to UV-A radiation [3]. This treatment is effective against, e.g., psoriasis and vitiligo [3]. In photopheresis, peripheral blood is the target of the photobiological action of psoralens in order to treat cutaneous T-cell lymphoma and other autoimmune disorders [3]. As some psoralens show antibacterial activity and also antiviral activity (among others against Herpes virus and HIV type-1 virus), another possible field of application for psoralens is the purification of blood and blood products [4].

During the last 40 years, much effort has been spent in photobiological, photochemical, and photophysical research on clarifying the underlying mechanisms of the desired phototherapeutical effects and undesired side effects of psoralens (for reviews see [1,2,5]). It has been found that these heterocyclic carbonyl compounds can undergo photocycloadditions to biomolecules such as DNA and RNA or unsaturated fatty acids [3]. In the case of DNA, the psoralen is assumed to be intercalated between the two DNA strands first [6]. After photoexcitation, it may form photocycloadducts to pyrimidine bases (most effectively to thymidine) involving the C=C double bond of the furan ring (2, 3-position, see Fig. 1), the C=C double bond of the pyrone ring (5, 6-position, see Fig. 1), or both [3,6]. In the latter case, the resulting cross-links between the two DNA

* Corresponding author. Tel.: +49 211 81 13209; fax: +49 211 81 13466.
E-mail address: christel.marian@uni-duesseldorf.de (C.M. Marian).

1010-6030/$ – see front matter © 2003 Elsevier B.V. All rights reserved.
doi:10.1016/j.jphotochem.2004.05.026

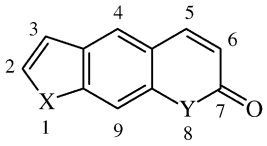

X,Y = O, S or Se

Fig. 1. Chemical structure of psoralens: in the parent compound: X = Y = O. In synthetic thio- and seleno-psoralens one or both of the intracyclic oxygen atoms is replaced by sulfur or selenium. We use the numbering for the parent compound throughout.

strands will inhibit the excessive mitosis of cells, causing a reduction of the proliferation which is characteristic, e.g., of psoriasis. This DNA reaction is also thought to be the active principle behind the antiviral and antibacterial activity of psoralens [5]. However, photoexcited psoralens may also take part in electron transfer reactions to molecular oxygen leading to the formation of superoxide ($O_2^{\odot -}$) or hydroxyl ($OH^{\odot}$) radicals (oxygen-dependent type I reactions) [7,8]. Additionally, they may produce singlet molecular oxygen O_2 ($^1\Delta_g$) via excitation energy transfer (oxygen-dependent type II reaction) [5,7,8].

As some of the possible photoreactions (e.g. the oxygen-dependent type I and II reactions) of psoralens may cause severe side effects, many synthetic psoralens have been developed in order to minimize these effects and optimize the phototherapeutical use [1,9,10]. Among them, sulfur and selenium analogs of psoralen (Fig. 1 and Table 1) show enhanced light absorption in the UV-A region (400–320 nm, often a wavelength of 365 nm is used in practice) compared to the parent psoralen [11]. For some of these compounds (especially 7H-thiopyrano [3,2-f] [1] benzofuran-7-one), a high DNA-photobinding ability has been observed [12]. As nucleic acid bases are known to quench psoralen triplet states effectively [13], it seems likely that the reaction of psoralens with DNA proceeds via a triplet excited state. Further evidence is given by the excited state lifetimes which are much longer for triplet states than for singlet ones [4]. Concerning the heteropsoralens (HPS), an enhancement of the singlet–triplet intersystem crossing (ISC) rates and triplet formation quantum yields due to the heavy atom effect is expected to be at least in part responsible for their increased reactivity. However, a definite answer to the question about the reacting state in the psoralen photocycloaddition to DNA is still missing (see, for example, Ref. [5]). For a similar discussion on the photodimerization of coumarin see Ref. [14].

Early spectroscopic studies of Song and coworkers on the parent psoralen (X = Y = O, Fig. 1) revealed a T_1 state of $\pi \rightarrow \pi^*$ type phosphorescing at $\lambda^P = 456$ nm with a life time of $\tau_P \approx 0.66$ s in ethanol at 77 K [15,16]. Fluorescence is observable in ethanol, too. However, the quantum yield of fluorescence ($\Phi_F \approx 0.019$) is much less than the one of phosphorescence ($\Phi_P \approx 0.13$) and the fluorescence band is very broad and shape-less. Mantulin and Song suspected an excited singlet state of $n \rightarrow \pi^*$ type near the lowest excited singlet state of $\pi \rightarrow \pi^*$ type to be involved in the fast radiationless depletion of the singlet $\pi \rightarrow \pi^*$ state to the electronic ground state S_0 [15]. Further studies on various psoralen derivatives, e.g. on 8-methoxypsoralen by Lim and coworkers [17], showed a strong dependence of the fluorescence quantum yield on the solvent and on the temperature. The same applies to the triplet formation quantum yield. More precisely, *both* the quantum yields of fluorescence and triplet formation were found to decrease with decreasing solvent polarity or proticity and with increasing temperature. Lim and coworkers introduced the term "proximity effect" and suggested vibronic coupling of the $S_1(\pi \rightarrow \pi^*)$ state with a nearby $S_2(n \rightarrow \pi^*)$ state via an out-of-plane bending mode to be responsible for this behavior [17,18].

The absorption, fluorescence emission, and triplet–triplet absorption spectra for five HPS in various solvents such as benzene, ethanol, and trifluoroethanol (TFE) were investigated by Aloisi et al. [4]. In addition, they studied the quantum yield of singlet-oxygen production after photoexcitation in aerated solution. From these data, rate constants and quantum yields for various radiative and non-radiative transitions were derived. Collet et al. studied the photosensitized generation of hydroxyl radicals in water by ESR spin trapping techniques [11]. They also presented absorption spectra for all heteropsoralens in water, ethanol and mixtures of both [11]. In addition, the efficiency of photobinding to DNA for various heteropsoralens was evaluated by Collet et al. [12].

Table 1
Nomenclature of sulfur and selenium analogs of psoralen

X	Y	Heteroanalogs	Abbreviation[a]
O	O	7H-furo [3,2-g] [1] benzopyran-7-one	PSO(O–O)
O	S	7H-thiopyrano [3,2-f] [1] benzofuran-7-one	PSO(O–S)
O	Se	7H-selenopyrano [3,2-f] [1] benzofuran-7-one	PSO(O–Se)
S	O	2H-thieno [3,2-g] [1] benzopyran-2-one	PSO(S–O)
Se	O	2H-selenolo [3,2-g] [1] benzopyran-2-one	PSO(Se–O)
S	S	7H-thieno [3,2-g] [1] benzothiopyran-7-one	PSO(S–S)
S	Se	7H-selenopyrano [3,2-f] [1] benzothiophen-7-one	PSO(S–Se)
Se	S	2H-selenolo [3,2-g] [1] benzothiopyran-2-one	PSO(Se–S)
Se	Se	7H-selenolo [3,2-g] [1] benzoselenopyran-7-one	PSO(Se–Se)

[a] Taken from Collet et al. [11].

So far, theoretical investigations on psoralen and its derivatives have been carried out solely by semiempirical methods [4] or time-dependent density functional theory (TD-DFT) [8,19]. The purpose of the current work is to elucidate mechanisms and trends in the photophysical properties of HPS utilizing more advanced quantum chemical methods. The questions to be dealt with are:

(1) What is the effect of the hetero-atom substitution on the vertical electronic excitation spectra and the capability of absorption in the UV-A region?
(2) Which spin–orbit matrix elements give rise to noticeable ISC from the singlet into the triplet manifold? How does spin–orbit coupling (SOC) between singlet and triplet states change when intracyclic oxygen is replaced by sulfur or selenium?
(3) Is there a pronounced dependence of electronic excitation energies on the solvent polarity? What are the consequences with respect to intersystem crossing channels which are accessible upon UV-A excitation?

2. Methods and computational details

For the computation of electronic excitation spectra, a quantum chemical method has to be applied which allows for a balanced description of static and dynamic electron correlation and which brings about high computational expense. In order to minimize the latter, we decided to determine the potential energy surface minima of the electronic ground states at the level of density functional theory (DFT). The vertical electronic excitation energies and the dipole (transition) matrix elements were obtained from subsequent single-point calculations applying the combined density functional theory/multi-reference configuration interaction (DFT/MRCI) approach of Grimme and Waletzke [20]. Spin–orbit matrix elements (SOMEs) for the correlated DFT/MRCI wavefunctions were computed using the spin–orbit coupling kit SPOCK which has recently been developed in our laboratory [21].

In Sections 2.1–2.4 below, details of the various computational procedures are given. Unless noted otherwise, C_s symmetry constraints were imposed and TZVP basis sets from the TURBOMOLE library [22] were applied. For the parent psoralen (X = Y = O), additional calculations with a second basis set including diffuse functions were carried out in order determine the energy regime of the lowest Rydberg states. This basis set called TZVP + Ryd consists of the original TZVP basis set and 3s, 3p, and 1d primitive diffuse Gaussians with origin at two dummy centers and exponents of 0.05, 0.02, 0.008 (s and p-Rydberg) and 0.015 (d-Rydberg). The two dummy centers were located inside the pyrone and the furan ring, respectively, and were allowed to adjust during the geometry optimization. The introduction of a third dummy center inside the central benzene ring was not found to change the results noticeably.

2.1. Geometry optimization

For the electronic ground states, geometry optimizations were performed applying the restricted Kohn–Sham DFT algorithm of the TURBOMOLE 5.6 program package [23]. The B3-LYP functional was used [24,25]. Harmonic vibrational frequencies were calculated analytically at the resulting geometries to ensure that they correspond to true minima of the potential energy surface. Utilizing the TZVP+Ryd basis set for the parent psoralen, a numerical grid, usually employed for the cesium atom, was chosen for the quadrature of the exchange correlation potential at the dummy centers.

2.2. Electronic spectra

The DFT/MRCI method of Grimme and Waletzke represents a very efficient and accurate means to obtain spin-free electronic spectra for large organic systems (errors in excitation energy usually less than 0.3 eV) [20]. The principal idea is to include major parts of dynamic electron correlation by density functional theory whereas static correlation effects are taken into account by short MRCI expansions. This MRCI expansion is built up from a one-particle basis of Kohn–Sham orbitals employing the BH-LYP functional [26,27]. Molecular orbitals were generated using the TURBOMOLE 5.6 program package [23]. The MRCI expansion is kept short by extensive configuration selection. For further details concerning the DFT/MRCI method we refer to the original publication of Grimme and Waletzke [20].

We calculated 12 roots for the A′ and 8 roots for the A″ irreducible representation of the C_s symmetry group both for the singlet and the triplet multiplicity. Utilizing the TZVP basis set and applying standard selection thresholds, the dimension of the actual MRCI space ranged from approximately 1×10^5 to 7×10^5 configuration state functions (CSFs) per space and spin symmetry depending on the system under consideration. The size of the final reference space was approximately 100–200 CSFs per space and spin symmetry. Upon employing the TZVP + Ryd basis set for the parent psoralen, the dimension of the MRCI space was approximately 1.6×10^6 CSFs for the singlet case and 2.3×10^6 CSFs for the triplet case. The size of the reference space amounted to 100–130 CSFs, here.

2.3. Spin–orbit coupling

SOMEs in the basis of the DFT/MRCI wave-functions were computed using the recently developed SPOCK [21]. Key features of this program are: first, spin-coupling coefficients between CSFs for spin-dependent one-electron operators are determined fast [28]. Secondly, the one-center spin–orbit mean-field Hamiltonian is applied [29]. This non-empirical effective one-electron operator treats the expensive two-electron terms of the full Breit–Pauli Hamiltonian in a Fock-like manner [29]. The one-center approximation where the molecular mean-field is reduced to a sum

Table 2
Vertical electronic excitation energies ΔE (eV) and oscillatory strengths $f(r)$ for the parent psoralen PSO(O–O) (X = Y = O, see Fig. 1) at the optimized equilibrium geometry of the ground state S_0

State		DFT/MRCI [TZVP]				DFT/MRCI [TZVP + Ryd]		TDDFT [19], ΔE (eV)	Experiment, ΔE (eV)
		Dominant excitation(s)	c^2	ΔE (eV)	$f(r)$	ΔE (eV)	$f(r)$		
S_1	$2^1A'$	$\pi_H \rightarrow \pi^*_L$	0.75	3.81	0.168	3.81	0.166	3.77	3.76[a], 3.73[b], 3.70[c]
S_2	$1^1A''$	$n_{H-3} \rightarrow \pi^*_L$	0.66	4.24	≈0	4.21	≈0	4.40	
S_3	$3^1A'$	$\pi_{H-1} \rightarrow \pi^*_L$, $\pi_H \rightarrow \pi^*_{L+1}$	0.69, 0.12	4.48	0.299	4.48	0.276	4.36	4.19[b], 4.35[b], 4.51[b], 4.19[c]
S_4	$4^1A'$	$\pi \rightarrow \pi^*$ (mixed)		4.96	0.053	4.91	0.039	4.97	4.73[b]
S_5	$5^1A'$	$\pi_H \rightarrow \pi^*_{L+1}$, $\pi_{H-1} \rightarrow \pi^*_{L+1}$	0.55, 0.22	5.26	0.756	5.20	0.775	5.24	5.00[b], 5.14[b], 5.10[c]
S_6	$6^1A'$	$\pi_{H-2} \rightarrow \pi^*_L$, $\pi_{H-1} \rightarrow \pi^*_{L+2}$	0.43, 0.14	5.55	0.004	5.50	0.010	5.56	
S_7	$2^1A''$	–	–	–	–	5.50	0.003	–	
T_1	$1^3A'$	$\pi_{H-1} \rightarrow \pi^*_L$, $\pi_H \rightarrow \pi^*_L$	0.47, 0.33	2.95					
T_2	$2^3A'$	$\pi \rightarrow \pi^*$ (mixed)		3.28					
T_3	$3^3A'$	$\pi_H \rightarrow \pi^*_{L+1}$, $\pi_{H-1} \rightarrow \pi^*_L$	0.49, 0.19	3.79					
T_4	$1^3A''$	$n_{H-3} \rightarrow \pi^*_L$, $n_{H-3} \rightarrow \pi^*_{L+2}$	0.66, 0.12	4.08					
T_5	$4^3A'$	$\pi \rightarrow \pi^*$ (mixed)		4.37					
T_6	$5^3A'$	$\pi_{H-1} \rightarrow \pi^*_{L+1}$, $\pi_H \rightarrow \pi^*_{L+3}$	0.33, 0.20	4.56					
T_7	$6^3A'$	$\pi \rightarrow \pi^*$ (mixed)		4.61					

[a] From absorption in ethanol at 77 K [15].
[b] From absorption in cyclohexane [34] (multiple entries correspond to vibrational progressions).
[c] From absorption in water–ethanol (volume ratio 95:5) [11].

of atomic contributions brings about considerable additional computational savings. Originally devised for heavy-metal compounds [29], this one-center mean-field approximation proved to cause only minor errors even in the case of light organic molecules [30].

2.4. Solvent effects

For the parent psoralen, spectral shifts due to electrostatic interactions in polar solvents were estimated employing the conductor-like screening model (COSMO) which is implemented in the TURBOMOLE package [31,32]. Of course, hydrogen bonding cannot be taken into account properly this way. A dielectric constant of $\epsilon = 78.54$ corresponding to water at a temperature of 298 K was chosen [33]. Electronic excitation energies are taken from DFT/MRCI calculations in the one-particle basis of COSMO optimized Kohn–Sham orbitals utilizing the TZVP basis set. Because of technical reasons, C_1 symmetry had to be used. 14 roots were computed for both singlet and triplet multiplicity. The geometry of the ground state was reoptimized.

3. Results and discussion

3.1. Vertical electronic excitation spectra and characterization of the low-lying excited states

3.1.1. The parent compound

For the parent psoralen (X = Y = O, see Fig. 1), electronic excitation energies from TD-DFT calculations applying the B3-LYP functional have recently been reported by Llano et al. [8] and Nakata et al. [19]. Nevertheless, we discuss the vertical electronic excitation spectrum of the parent psoralen in some detail here, because this will pave the way for a discussion of the spectral changes occurring when sulfur or selenium is substituted for intracyclic oxygen. The vertical singlet and triplet spectra obtained from DFT/MRCI

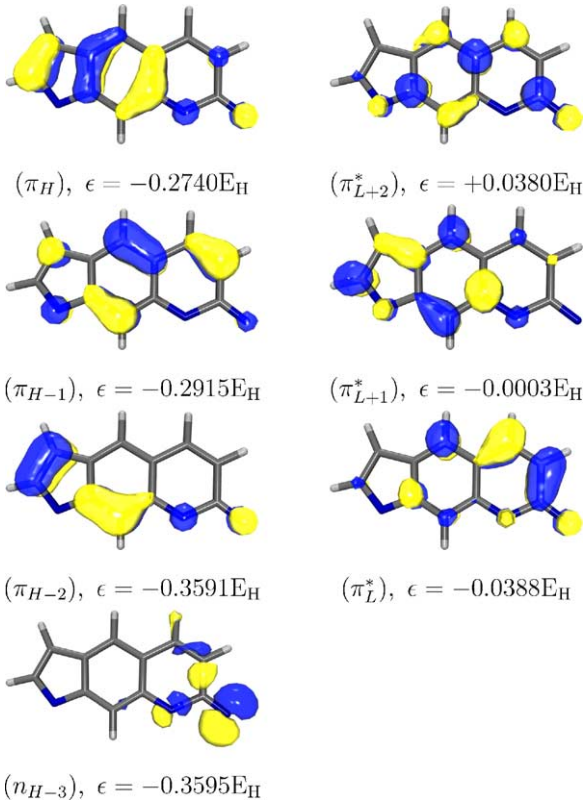

Fig. 2. The highest occupied and lowest unoccupied Kohn–Sham MOs for psoralen PSO(O–O) (X = Y = O, see Fig. 1. S_0 geometry, BH-LYP functional, TZVP basis, isoline = 0.050.)

computations together with the TD-DFT values from Ref. [19] and some experimental absorption maxima from Refs. [15,34] are shown in Table 2.

The valence molecular orbitals which are involved in the dominant excitations listed in Table 2 are depicted in Fig. 2. With respect to the location of nodal planes, these valence molecular orbitals are in close agreement with those presented by Nakata et al. [19]. The lone-pair orbital (denoted n_{H-3} in Fig. 2) is localized almost exclusively around the carbonyl group of the pyrone ring. The occupied orbital π_{H-1} is completely delocalized and is bonding in the region of the 5–6 double bond in the pyrone ring. The highest occupied molecular orbital (HOMO, denoted π_H in Fig. 2) is mainly located at the furan side and the benzene ring. It is bonding with respect to the 2–3 double bond. The lowest unoccupied molecular orbital (LUMO, denoted π^*_L in Fig. 2) has major contributions in the pyrone ring and is antibonding with respect to the 5–6 double bond. The centroid of the virtual orbital π^*_{L+1} is (like that of the orbital π_H) directed towards the furan ring, but π^*_{L+1} is antibonding with respect to the 2–3 double bond. The 2–3 and the 5–6 double bonds are involved in the [2 + 2]-photocycloaddition reactions of psoralens to DNA bases.

At the equilibrium geometry of the ground state, our calculations predict the lowest-lying singlet excited state S_1 to be the $2^1A'$ state of $\pi \rightarrow \pi^*$ character. The dominant configuration for this state ($\pi_H \rightarrow \pi^*_L$) corresponds to the HOMO–LUMO transition. Our computed excitation energy of 3.81 eV is in excellent agreement with the experimental absorption maximum at 3.73 eV in cyclohexane [34] and the theoretical value of 3.77 eV obtained by Nakata et al. [19]. The S_2 state corresponds to the $n_{H-3} \rightarrow \pi^*_L$ excitation. Energetically, it is located at 4.24 eV, in good accord with the value 4.40 eV given in Ref. [19]. The TD-DFT calculations of Nakata et al., however, predict it to be the third excited singlet state, slightly above another $\pi \rightarrow \pi^*$ excited state [19]. In our calculations, the latter state appears as S_3 at 4.48 eV. Both the S_1 and S_3 $\pi \rightarrow \pi^*$ excited states show a middle-sized oscillatory strength. Due to the energetic location, the practically important absorption in the UV-A region ranging from 320 to 400 nm may be addressed solely to S_1. At higher energies of ≈5 eV, a strongly absorbing state is found in experiment [34]. We assign the transition between S_0 and $S_5(5^1A')$ at 5.26 eV with an oscillatory strength of 0.756 to this band. The energy of this $\pi \rightarrow \pi^*$ excitation is almost unchanged by the inclusion of diffuse functions in the basis set, confirming that it is a pure valence-type state.

In the triplet manifold, there are three states (T_1–T_3) of $\pi \rightarrow \pi^*$ character in the vertical spectrum with energies below the first excited singlet state S_1. As expected, the singlet–triplet splitting is much larger for the $\pi \rightarrow \pi^*$ excited states than for the $n \rightarrow \pi^*$ excited states. The $n_{H-3} \rightarrow \pi^*_L$ excited triplet state $T_4(1^3A'')$ is located above S_1 and only slightly below the corresponding singlet $n \rightarrow \pi^*$ state $S_2(1^1A'')$.

Remarkably, the spatial wave functions of the $\pi \rightarrow \pi^*$ excited triplet states differ considerably from their singlet counterparts. The lowest excited triplet state T_1 is not dominated by the HOMO–LUMO transition $\pi_H \rightarrow \pi^*_L$, in contrast to S_1. Instead, it shows strong mixing of the configurations $\pi_H \rightarrow \pi^*_L$ and $\pi_{H-1} \rightarrow \pi^*_L$. From the shape of the MOs involved in the low-lying $\pi \rightarrow \pi^*$ transitions, one would assign a sizeable shift of electronic charge towards the pyrone ring and a reduction in bond strength both for the 2–3 and the 5–6 double bonds to the S_1 state. The charge displacement should be much less in the T_1 state for which a strong reduction in bond order in the 5–6 double bond but almost no change in the 2–3 double bond is expected.

Table 3
Vertical electronic excitation energies ΔE (eV) and oscillatory strength $f(r)$ for singlet states in parentheses for mono-substituted heteropsoralens (DFT/MRCI, TZVP basis, equilibrium geometry of the ground state)

State	X = O, Y = S	X = O, Y = Se	X = S, Y = O	X = Se, Y = O[a]
S_1	$2^1A'$ ($\pi \rightarrow \pi^*$)	$2^1A'$ ($\pi \rightarrow \pi^*$)	$2^1A'$ ($\pi \rightarrow \pi^*$)	$2^1A'$ ($\pi \rightarrow \pi^*$)
	3.45 (0.081)	3.25 (0.059)	3.65 (0.028)	3.58 (0.005)
S_2	$1^1A''$ ($n \rightarrow \pi^*$)	$1^1A''$ ($n \rightarrow \pi^*$)	$3^1A'$ ($\pi \rightarrow \pi^*$)	$3^1A'$ ($\pi \rightarrow \pi^*$)
	3.62 (≈0)	3.44 (2×10^{-4})	4.18 (0.370)	4.03 (0.340)
S_3	$3^1A'$ ($\pi \rightarrow \pi^*$)	$3^1A'$ ($\pi \rightarrow \pi^*$)	$1^1A''$ ($n \rightarrow \pi^*$)	$1^1A''$ ($n \rightarrow \pi^*$)
	4.16 (0.107)	4.06 (0.080)	4.22 (3×10^{-4})	4.23 (3×10^{-4})
S_4	$4^1A'$ ($\pi \rightarrow \pi^*$)	$4^1A'$ ($\pi \rightarrow \pi^*$)	$4^1A'$ ($\pi \rightarrow \pi^*$)	$2^1A''$ ($\pi \rightarrow \sigma^*$)
	4.52 (0.076)	4.35 (0.067)	4.64 (0.315)	4.32 (≈0)
S_5	$5^1A'$ ($\pi \rightarrow \pi^*$)	$5^1A'$ ($\pi \rightarrow \pi^*$)	$5^1A'$ ($\pi \rightarrow \pi^*$)	$4^1A'$ ($\pi \rightarrow \pi^*$)
	4.83 (0.741)	4.65 (0.639)	5.02 (0.645)	4.49 (0.454)
T_1	$1^3A'$ ($\pi \rightarrow \pi^*$)	$1^3A'$ ($\pi \rightarrow \pi^*$)	$1^3A'$ ($\pi \rightarrow \pi^*$)	$1^3A'$ ($\pi \rightarrow \pi^*$)
	2.85	2.78	2.91	2.87
T_2	$2^3A'$ ($\pi \rightarrow \pi^*$)	$2^3A'$ ($\pi \rightarrow \pi^*$)	$2^3A'$ ($\pi \rightarrow \pi^*$)	$2^3A'$ ($\pi \rightarrow \pi^*$)
	3.13	3.02	3.16	3.15
T_3	$3^3A'$ ($\pi \rightarrow \pi^*$)	$1^3A''$ ($n \rightarrow \pi^*$)	$3^3A'$ ($\pi \rightarrow \pi^*$)	$3^3A'$ ($\pi \rightarrow \pi^*$)
	3.45	3.29	3.53	3.38
T_4	$1^3A''$ ($n \rightarrow \pi^*$)	$3^3A'$ ($\pi \rightarrow \pi^*$)	$1^3A''$ ($n \rightarrow \pi^*$)	$1^3A''$ ($\pi \rightarrow \sigma^*$)
	3.47	3.34	4.05	4.04

[a] The $n \rightarrow \pi^*$ type state $2^3A''$ corresponds to T_6 and is located at 4.06 eV. The T_5 state at 4.05 eV originates from a $\pi \rightarrow \pi^*$ excitation.

Table 4
Vertical electronic excitation energies ΔE (eV) and oscillatory strength $f(r)$ for singlet states in parentheses for di-substituted heteropsoralens (DFT/MRCI, TZVP basis, equilibrium geometry of the ground state)

State	X = S, Y = S	X = S, Y = Se	X = Se, Y = S[a]	X = Se, Y = Se[b]
S_1	$2^1A'$ ($\pi \rightarrow \pi^*$)	$2^1A'$ ($\pi \rightarrow \pi^*$)	$2^1A'$ ($\pi \rightarrow \pi^*$)	$2^1A'$ ($\pi \rightarrow \pi^*$)
	3.34 (0.024)	3.15 (0.027)	3.29 (0.013)	3.12 (0.022)
S_2	$1^1A''$ (n $\rightarrow \pi^*$)	$1^1A''$ (n $\rightarrow \pi^*$)	$1^1A''$ (n $\rightarrow \pi^*$)	$1^1A''$ (n $\rightarrow \pi^*$)
	3.58 ($\approx$0)	3.41 (2×10^{-4})	3.58 ($\approx$0)	3.41 (2×10^{-4})
S_3	$3^1A'$ ($\pi \rightarrow \pi^*$)	$3^1A'$ ($\pi \rightarrow \pi^*$)	$3^1A'$ ($\pi \rightarrow \pi^*$)	$3^1A'$ ($\pi \rightarrow \pi^*$)
	3.95 (0.218)	3.85 (0.188)	3.85 (0.229)	3.75 (0.214)
S_4	$4^1A'$ ($\pi \rightarrow \pi^*$)	$4^1A'$ ($\pi \rightarrow \pi^*$)	$4^1A'$ ($\pi \rightarrow \pi^*$)	$4^1A'$ ($\pi \rightarrow \pi^*$)
	4.31 (0.142)	4.19 (0.076)	4.19 (0.234)	4.09 (0.152)
S_5	$5^1A'$ ($\pi \rightarrow \pi^*$)	$5^1A'$ ($\pi \rightarrow \pi^*$)	$2^1A''$ ($\pi \rightarrow \sigma^*$)	$2^1A''$ ($\pi \rightarrow \sigma^*$)
	4.67 (0.798)	4.53 (0.770)	4.21 ($\approx$0)	4.17 ($\approx$0)
T_1	$1^3A'$ ($\pi \rightarrow \pi^*$)	$1^3A'$ ($\pi \rightarrow \pi^*$)	$1^3A'$ ($\pi \rightarrow \pi^*$)	$1^3A'$ ($\pi \rightarrow \pi^*$)
	2.82	2.75	2.80	2.73
T_2	$2^3A'$ ($\pi \rightarrow \pi^*$)	$2^3A'$ ($\pi \rightarrow \pi^*$)	$2^3A'$ ($\pi \rightarrow \pi^*$)	$2^3A'$ ($\pi \rightarrow \pi^*$)
	2.97	2.85	2.95	2.83
T_3	$3^3A'$ ($\pi \rightarrow \pi^*$)	$3^3A'$ ($\pi \rightarrow \pi^*$)	$3^3A'$ ($\pi \rightarrow \pi^*$)	$3^3A'$ ($\pi \rightarrow \pi^*$)
	3.28	3.21	3.20	3.15
T_4	$1^3A''$ (n $\rightarrow \pi^*$)	$1^3A''$ (n $\rightarrow \pi^*$)	$1^3A''$ (n $\rightarrow \pi^*$)	$1^3A''$ (n $\rightarrow \pi^*$)
	3.41	3.25	3.41	3.24

[a] $5^1A'$ ($\pi \rightarrow \pi^*$) at 4.59 eV with an oscillatory strength of 0.738.
[b] $5^1A'$ ($\pi \rightarrow \pi^*$) at 4.48 eV with an oscillatory strength of 0.754.

Actually, the characterization of T_1 as a strongly localized diradical in the 5, 6-positions in the pyrone ring was already postulated by Song and coworkers in the early 1970s [15].

The different localization of electronic charge in the excited states brings about large differences in the excited state dipole moments (see Table 6). The dipole moment of the ground state S_0 amounts to 6.23 D, pointing from the furan ring towards the carbonyl group. Whereas the dipole moment of S_1 (8.66 D) is considerably increased with respect to the ground state value, this is not the case for the T_1 state (5.77 D). For the $n_{H-3} \rightarrow \pi^*_L$ excited states S_2 and T_4, a shift of charge towards the furan ring results in a strong reduction of the dipole moment to 1.23 D. For the high-lying $\pi \rightarrow \pi^*$ excited state S_5, a relatively moderate increase of the dipole moment compared to S_1 is observed, corresponding to a value of 7.21 D.

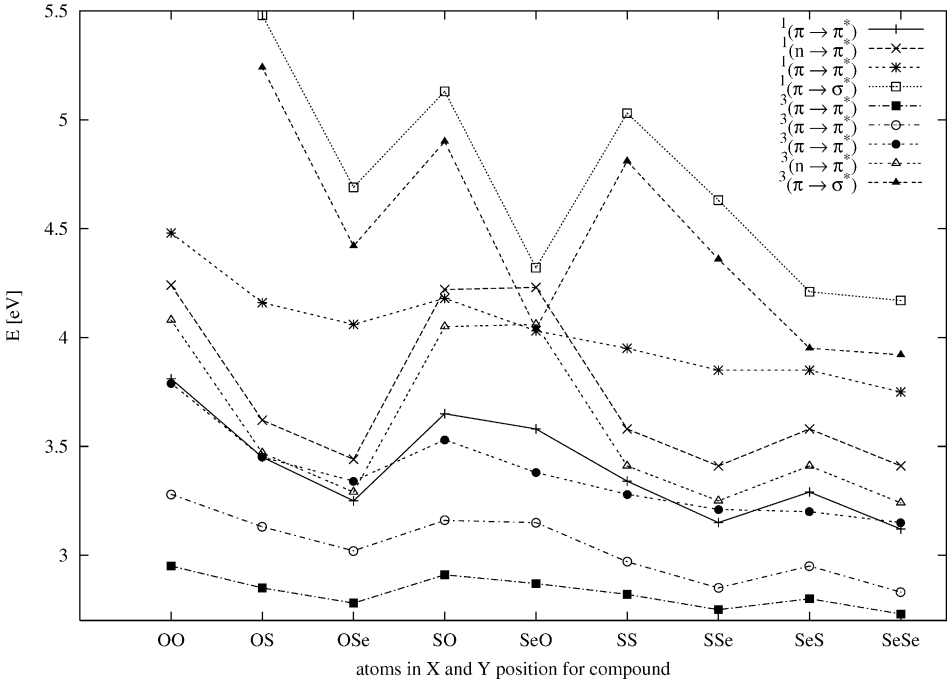

Fig. 3. Vertical excitation energies ΔE (eV) of heteropsoralens at the equilibrium geometry of the ground state S_0. (Abscissa encoding corresponding to Fig. 1. DFT/MRCI, TZVP basis, higher-lying states of $\pi \rightarrow \pi^*$ type are ommitted.)

3.1.2. Thio- and seleno-psoralens

For the mono- and di-substituted heteropsoralens, the vertical electronic excitation spectra are given in Tables 3 and 4, respectively. In addition, the excitation energies are represented graphically in Fig. 3.

A look at Fig. 3 reveals that the hetero-atom substitution in Y position has a large effect on the excitation energy of the singlet and triplet excited states of $n \rightarrow \pi^*$ character. In contrast, substitution in the X position does not introduce any noticeable change in the excitation energy of these states. For example, in PSO(O–Se) (X = O, Y = Se) the vertical excitation energy of the $n \rightarrow \pi^*$ type state $1^1A''$ is lowered by 0.80 eV compared to the parent psoralen whereas in PSO(Se–O) (X = Se, Y = O) this state is found at the same energy as in the parent psoralen. These findings are obviously related to the facts that the n orbital is strongly localized at the carbonyl group and that the LUMO π_L^* has only minor contributions in the 1-position at the furan side.

In contrast, the vertical excitation energy of the T_1 state, being of $\pi \rightarrow \pi^*$ type in all cases, is remarkably constant. For all the psoralens under study, this behavior supports the view of T_1 as a diradicaloid state which is localized in the 5–6 double bond of the pyrone moiety and is therefore nearly unaffected by hetero-atom substitution. In the S_1 state more prominent changes occur, in particular upon substitution in the six-membered pyrone ring. This state is appreciably lowered in excitation energy upon hetero-atom substitution (up to 0.69 eV for X = Y = Se). The different behaviors of S_1 and T_1 may be taken as an indication that, similar to the situation for the parent psoralen, the electronic structure of the S_1 state is more ionic than that of the T_1 state for all these psoralens.

In Table 5, data of the experimental absorption spectra for all HPS in a water–ethanol mixture are given together with a tentative assignment of the bands to our computed electronic transitions. The experimental data are taken from the work of Collet et al. [11] Our calculated excitation energies are in very good agreement with the experimental values. A maximum deviation of 0.31 eV is recognized in the case of the $S_0 \rightarrow S_3$ transition for PSO(O–S). For the parent psoralen and its analogs which are hetero-substituted at the pyrone side only, we assign the lowest $\pi \rightarrow \pi^*$ singlet states with moderate oscillatory strengths to long-wavelength shoulders given by Collet et al. For all psoralens which contain sulfur or selenium inside the five-membered ring, however, the lowest-lying singlet $\pi \rightarrow \pi^*$ states show very low oscillatory strengths (<0.03). For these compounds, we suggest the first pronounced band to result from an excitation of the second $\pi \rightarrow \pi^*$ excited state, whereas the lowest-lying $\pi \rightarrow \pi^*$ states may be associated to the broad long-wavelength tails appearing in the experimental spectra. Concerning practical application in PUVA, the marginal intensity of the $S_0 \rightarrow S_1$ transition has not necessarily to be a major drawback. Sufficient absorption in the UV-A region may be provided by the second $\pi \rightarrow \pi^*$ excited singlet states which are lowered in energy upon disubstitution down to 3.75–3.95 eV according to our calculations (Tables 3 and 4).

Quite remarkably, in the vertical spectra of all heterosubstituted psoralens, we find additional states of A'' symmetry in the energy regime below 5.5 eV that do not result

Table 5
Wavelengths λ_{max} of experimental absorption maxima and corresponding extinction coefficients ϵ in water–ethanol (volume ratio 95:5) taken from Collet et al. [11] and assignment to our calculated gas phase transitions[a]

X	Y	λ_{max} (nm)	ΔE_{obs} (eV)	ϵ ($dm^3\,mol^{-1}\,cm^{-1}$)	Assignment	ΔE_{calc} (eV)	$f(r)$
O	O	335[b]	(3.70)	7600	$S_0 \rightarrow S_1$	3.81	0.168
		296	(4.19)	13900	$S_0 \rightarrow S_3$	4.48	0.299
		(243)	(5.10)		$S_0 \rightarrow S_5$	5.26	0.756
O	S	365[b]	(3.40)	3300	$S_0 \rightarrow S_1$	3.45	0.081
		322	(3.85)	9700	$S_0 \rightarrow S_3$	4.16	0.107
		(259)	(4.79)		$S_0 \rightarrow S_5$	4.83	0.741
O	Se	375[b]	(3.31)	2700	$S_0 \rightarrow S_1$	3.25	0.059
		323	(3.84)	9100	$S_0 \rightarrow S_3$	4.06	0.080
		(261)	(4.75)		$S_0 \rightarrow S_5$	4.65	0.639
S	O	316	(3.92)	13500	$S_0 \rightarrow S_2$	4.18	0.370
		(272)	(4.56)		$S_0 \rightarrow S_4$	4.64	0.315
S	S	336	(3.69)	10600	$S_0 \rightarrow S_3$	3.95	0.218
		(296)	(4.19)		$S_0 \rightarrow S_4$	4.31	0.142
S	Se	337	(3.68)	12000	$S_0 \rightarrow S_3$	3.85	0.188
		(295)	(4.20)		$S_0 \rightarrow S_4$	4.19	0.076
Se	O	323	(3.84)	13600	$S_0 \rightarrow S_2$	4.03	0.340
		(280)	(4.43)		$S_0 \rightarrow S_5$	4.49	0.454
Se	S	342	(3.63)	10500	$S_0 \rightarrow S_3$	3.85	0.229
		(298)	(4.16)		$S_0 \rightarrow S_4$	4.19	0.234
Se	Se	343	(3.62)	9900	$S_0 \rightarrow S_3$	3.75	0.214
		(301)	(4.12)		$S_0 \rightarrow S_4$	4.09	0.152

[a] In parentheses, we give the corresponding excitation energies ΔE_{obs} and some additional approximate values for absorption maxima beyond the UV-A region which we obtained from the plotted spectra published by Collet et al.

[b] Shoulder.

Table 6
Dipole moments μ [D] of ground and excited states for mono-substituted heteropsoralens (DFT/MRCI, TZVP basis, equilibrium geometry of the ground state)

State	Dipole moments (μ)									
	X = O, Y = O		X = O, Y = S		X = O, Y = Se		X = S, Y = O		X = Se, Y = O[a]	
S_0	X^1A'	6.23	X^1A'	6.11	X^1A'	5.82	X^1A'	5.90	X^1A'	5.80
S_1	$2^1A'$	8.66	$2^1A'$	7.85	$2^1A'$	7.08	$2^1A'$	9.56	$2^1A'$	10.44
S_2	$1^1A''$	1.23	$1^1A''$	2.12	$1^1A''$	2.15	$3^1A'$	10.78	$3^1A'$	10.98
S_3	$3^1A'$	9.92	$3^1A'$	8.64	$3^1A'$	8.08	$1^1A''$	1.22	$1^1A''$	1.16
S_4	$4^1A'$	6.77	$4^1A'$	5.45	$4^1A'$	5.60	$4^1A'$	6.30	$2^1A''$	6.37
S_5	$5^1A'$	7.21	$5^1A'$	5.60	$5^1A'$	4.26	$5^1A'$	5.21	$4^1A'$	6.60
T_1	$1^3A'$	5.77	$1^3A'$	5.97	$1^3A'$	6.02	$1^3A'$	5.81	$1^3A'$	6.04
T_2	$2^3A'$	7.45	$2^3A'$	7.24	$2^3A'$	6.85	$2^3A'$	8.03	$2^3A'$	8.15
T_3	$3^3A'$	7.88	$3^3A'$	6.57	$1^3A''$	2.01	$3^3A'$	7.11	$3^3A'$	7.15
T_4	$1^3A''$	1.23	$1^3A''$	1.97	$3^3A'$	5.29	$1^3A''$	1.30	$1^3A''$	6.22

[a] Here, the states $1^3A''$ and $2^1A''$ are of $\pi \rightarrow \sigma^*$ type. $2^3A''$ (not shown) is of $n \rightarrow \pi^*$ type.

from $n \rightarrow \pi^*$ excitations. These states correspond to single excitations from π-type MOs into virtual MOs of A′ symmetry which we denote by σ^* in order to emphasize that they are valence like and not Rydberg like. The singlet–triplet splitting for these states is small (around 0.2–0.3 eV). The occurrence of states of this type at low excitation energies can be related to the questions of photostability and photoreactivity of the psoralens. The lowest excitation energies (4.17 eV for the singlet and 3.92 for the triplet) of $\pi \rightarrow \sigma^*$ excited states are obtained for PSO(Se–Se). For PSO(Se–O), our calculations predict the lowest excited triplet state of A″ symmetry to be of $\pi \rightarrow \sigma^*$ type with an excitation energy of 4.04 eV below the nearly degenerate $2^3A''$ state of $n \rightarrow \pi^*$ type at 4.06 eV. In the case of PSO(O–Se), however, the lowest excited triplet state of $\pi \rightarrow \sigma^*$ type is located considerably higher at 4.42 eV. Thus, psoralens which contain selenium in the furan ring are expected to be least photostable in accord with chemical intuition. In the case of the parent psoralen, the lowest singlet state corresponding to an excitation from a π-type orbital into an orbital of A′ symmetry ($2^1A''$ at 5.50 eV employing the TZVP + Ryd basis set) is of s-Rydberg type at the ground state equilibrium geometry.

3.2. Solvent effects

Excitation energies of the parent compound in aqueous solution as mimicked by the COSMO solvation model are displayed in Table 8. The most pronounced changes compared to the vacuum values are observed for the $n \rightarrow \pi^*$ states. They are blue-shifted by 0.48 eV. For the $\pi \rightarrow \pi^*$ excited singlet state S_3, a red shift of 0.11 eV is obtained. Comparing the experimental absorption maxima in cyclohexane (median of vibrational progression at 4.35 eV, [34]) and water–ethanol mixtures (band maximum at 4.19 eV, [11]), an experimental estimate of 0.16 eV may be extracted for the bathochromic shift of the $S_0 \rightarrow S_3$ transition. The effect of solvation on the energy of the other $\pi \rightarrow \pi^*$ states is almost negligible within this model. In a simplified picture, the energetic stabilization or destabilization of the ground and excited states in polar solvents is connected to their dipole moments and the extent of polarization they induce in the surrounding solvent. Compared to the electronic ground state, the $n \rightarrow \pi^*$ states show dramatically reduced dipole moments. The dipole moment of the $\pi \rightarrow \pi^*$ state S_3 is noticeably increased, explaining the

Table 7
Dipole moments μ [D] of ground and excited states for di-substituted heteropsoralens (DFT/MRCI, TZVP basis, equilibrium geometry of the ground state)

State	Dipole moments (μ)							
	X = S, Y = S		X = S, Y = Se		X = Se, Y = S[a]		X = Se, Y = Se[b]	
S_0	X^1A'	5.78	X^1A'	5.51	X^1A'	5.72	X^1A'	5.45
S_1	$2^1A'$	8.31	$2^1A'$	7.28	$2^1A'$	8.92	$2^1A'$	7.73
S_2	$1^1A''$	1.64	$1^1A''$	1.62	$1^1A''$	1.49	$1^1A''$	1.54
S_3	$3^1A'$	10.31	$3^1A'$	9.96	$3^1A'$	11.05	$3^1A'$	10.91
S_4	$4^1A'$	5.36	$4^1A'$	5.25	$4^1A'$	5.96	$4^1A'$	5.51
S_5	$5^1A'$	4.10	$5^1A'$	2.62	$2^1A''$	5.44	$2^1A''$	4.93
T_1	$1^3A'$	5.57	$1^3A'$	5.39	$1^3A'$	5.62	$1^3A'$	5.34
T_2	$2^3A'$	8.49	$2^3A'$	7.76	$2^3A'$	9.35	$2^3A'$	8.54
T_3	$3^3A'$	5.87	$3^3A'$	4.88	$3^3A'$	5.65	$3^3A'$	4.83
T_4	$1^3A''$	1.55	$1^3A''$	1.52	$1^3A''$	1.41	$1^3A''$	1.45

[a] Dipole moment of S_6 ($5^1A'$): 3.43 D.
[b] Dipole moment of S_6 ($5^1A'$): 2.43 D.

Table 8
Simulated electronic spectrum for psoralen PSO(O–O) assuming a solvent polarity corresponding to water ($\epsilon = 78.54$) using COSMO: vertical excitation energies ΔE (eV) and oscillatory strengths $f(r)$ (DFT/MRCI, TZVP basis, equilibrium geometry of the ground state reoptimized with COSMO)

State	Symmetry	Type	ΔE	$f(r)$
S_0	X^1A'			
S_1	$2^1A'$	$\pi \rightarrow \pi^*$	3.80	0.140
S_2	$3^1A'$	$\pi \rightarrow \pi^*$	4.37	0.381
S_3	$1^1A''$	$n \rightarrow \pi^*$	4.72	2×10^{-4}
S_4	$4^1A'$	$\pi \rightarrow \pi^*$	4.96	0.055
S_5	$5^1A'$	$\pi \rightarrow \pi^*$	5.30	0.636
S_6	$6^1A'$	$\pi \rightarrow \pi^*$	5.57	0.016
S_7	$7^1A'$	$\pi \rightarrow \pi^*$	5.71	0.083
T_1	$1^3A'$	$\pi \rightarrow \pi^*$	3.00	
T_2	$2^3A'$	$\pi \rightarrow \pi^*$	3.28	
T_3	$3^3A'$	$\pi \rightarrow \pi^*$	3.79	
T_4	$4^3A'$	$\pi \rightarrow \pi^*$	4.39	
T_5	$1^3A''$	$n \rightarrow \pi^*$	4.56	
T_6	$5^3A'$	$\pi \rightarrow \pi^*$	4.59	
T_7	$6^3A'$	$\pi \rightarrow \pi^*$	4.68	
T_8	$7^3A'$	$\pi \rightarrow \pi^*$	5.31	
T_9	$8^3A'$	$\pi \rightarrow \pi^*$	5.66	

calculated red-shift in polar solvents. The absence of any noticeable bathochromic shift for the other $\pi \rightarrow \pi^*$ excited states in our calculation is consistent with their moderately changed dipole moments compared to the ground state.

The dipole moments for the ground and low-lying excited states of all the HPS are shown in Tables 6 and 7. They are comparable to the corresponding ones for the parent psoralen. In a first approximation, we thus expect the solvent effects for these compounds to be very similar to the above findings. Remarkably, the dipole moments of the $\pi \rightarrow \sigma^*$ states ($2^1A''$ and $1^3A''$ for PSO(Se–O)), are somewhat larger than the ground state value.

3.3. Spin–orbit coupling

For the psoralens under investigation, SOMEs which were computed at the ground state equilibrium geometries are listed in Tables 9 and 10. We restrict our presentation to matrix elements between low-lying singlet and triplet states which may thus be important for intersystem crossing processes following photoexcitation in the UV-A region. For showing up trends, the matrix elements are also depicted in Fig. 4.

For all psoralens under investigation, the tabulated SOMEs between a triplet and a singlet $\pi \rightarrow \pi^*$ excited state as well as SOMEs between a triplet $\pi \rightarrow \pi^*$ state and the ground state do not exceed 1–2 cm^{-1} and are often much less. On the other hand, the singlet–triplet coupling between a state of A′ symmetry and a state of A″ symmetry typically is in the order of several tens per centimeter to several hundreds per centimeter. This applies to $n \rightarrow \pi^*/\pi \rightarrow \pi^*$ couplings, to those ones between $n \rightarrow \pi^*$ triplet states and the ground state S_0, and also to couplings between $\pi \rightarrow \sigma^*$ excited states and states of A′ symmetry. The observed proportions of $n \rightarrow \pi^*/\pi \rightarrow \pi^*$, $\pi \rightarrow \pi^*/\pi \rightarrow \pi^*$, and $n \rightarrow \pi^*/n \rightarrow \pi^*$ couplings are widespread in organic photophysics and are known as El-Sayed's rules [35].

Large changes in SOMEs are expected upon hetero-atom substitution because the atomic SOC constants increase strongly with the nuclear charge [36]. It becomes immediately evident from a look at Fig. 4 that the substitution of selenium for an intracyclic oxygen atom of the parent psoralen can cause an enormous increase of the SOMEs, indeed. Replacement of oxygen by sulfur causes less dramatic effects on the SOMEs and their order of magnitude is roughly the same as for the parent psoralen. More precisely, the extent of change in the singlet–triplet coupling which is induced by selenium substitution depends on the pair of states under consideration and the site of substitution (furan or pyrone moiety). Selenium substitution in the 8-position

Table 9
Spin–orbit matrix elements (absolute values) [cm^{-1}] of the lowest singlet and triplet states for the parent psoralen and mono-substituted heteropsoralens (DFT/MRCI, TZVP basis, equilibrium geometry of the ground state. The component of the spin–orbit Hamiltonian is indicated in parentheses.)

	X = O, Y = O	X = O, Y = S	X = O, Y = Se	X = S, Y = O	X = Se, Y = O[a]
$\langle 1^3A'\|\mathcal{H}_{SO}\|X^1A'\rangle$	5×10^{-2} (z)	4×10^{-2} (z)	1.3 (z)	4×10^{-2} (z)	0.4 (z)
$\langle 1^3A'\|\mathcal{H}_{SO}\|2^1A'\rangle$	7×10^{-3} (z)	4×10^{-2} (z)	0.2 (z)	1×10^{-2} (z)	0.3 (z)
$\langle 2^3A'\|\mathcal{H}_{SO}\|2^1A'\rangle$	5×10^{-3} (z)	8×10^{-2} (z)	0.3 (z)	2×10^{-2} (z)	0.2 (z)
$\langle 3^3A'\|\mathcal{H}_{SO}\|2^1A'\rangle$	5×10^{-3} (z)	2×10^{-2} (z)	0.4 (z)	4×10^{-2} (z)	0.3 (z)
$\langle 1^3A''\|\mathcal{H}_{SO}\|X^1A'\rangle$	41.5 (x)/27.9 (y)	70.5 (x)/34.6 (y)	209.5 (x)/92.2 (y)	39.6 (x)/29.6 (y)	282.1 (x)/565.3 (y)
$\langle 1^3A''\|\mathcal{H}_{SO}\|2^1A'\rangle$	9.8 (x)/2.9 (y)	24.1 (x)/26.2 (y)	277.1 (x)/171.7 (y)	6.2 (x)/0.4 (y)	47.9 (x)/106.7 (y)
$\langle 1^3A''\|\mathcal{H}_{SO}\|3^1A'\rangle$	10.8 (x)/6.7 (y)	9.6 (x)/2.6 (y)	2.9 (x)/4.3 (y)	10.5 (x)/9.2 (y)	2.3 (x)/19.9 (y)
$\langle 1^3A'\|\mathcal{H}_{SO}\|1^1A''\rangle$	24.7 (x)/13.4 (y)	9.1 (x)/6.4 (y)	168.4 (x)/106.5 (y)	21.3 (x)/14.7 (y)	19.2 (x)/22.8 (y)
$\langle 2^3A'\|\mathcal{H}_{SO}\|1^1A''\rangle$	4.2 (x)/0.3 (y)	25.8 (x)/21.6 (y)	202.9 (x)/113.2 (y)	11.0 (x)/3.6 (y)	11.3 (x)/0.4 (y)
$\langle 3^3A'\|\mathcal{H}_{SO}\|1^1A''\rangle$	0.8 (x)/1.9 (y)	26.1 (x)/19.9 (y)	127.1 (x)/70.5 (y)	0.4 (x)/2.4 (y)	0.5 (x)/8.4 (y)
$\langle 1^3A''\|\mathcal{H}_{SO}\|1^1A''\rangle$	9×10^{-2} (z)	0.3 (z)	0.4 (z)	0.1 (z)	0.2 (z)
$\langle 2^3A''\|\mathcal{H}_{SO}\|X^1A'\rangle$	15.5 (x)/7.2 (y)	27.8 (x)/125.6 (y)	197.7 (x)/621.8 (y)	38.9 (x)/114.3 (y)	41.3 (x)/20.0 (y)

[a] Here, the state $1^3A''$ is of $\pi \rightarrow \sigma^*$ type. $2^3A''$ is of $n \rightarrow \pi^*$ type.

Table 10
Spin–orbit matrix elements (absolute values) [cm^{-1}] of the lowest singlet and triplet states for di-substituted heteropsoralens (DFT/MRCI, TZVP basis, equilibrium geometry of the ground state. The component of the spin–orbit Hamiltonian is indicated in parentheses.)

	X = S, Y = S	X = S, Y = Se	X = Se, Y = S	X = Se, Y = Se
$\langle 1^3A'\|\mathcal{H}_{SO}\|X^1A'\rangle$	5×10^{-2} (z)	1.4 (z)	0.4 (z)	0.5 (z)
$\langle 1^3A'\|\mathcal{H}_{SO}\|2^1A'\rangle$	9×10^{-3} (z)	0.2 (z)	0.2 (z)	0.2 (z)
$\langle 2^3A'\|\mathcal{H}_{SO}\|2^1A'\rangle$	8×10^{-2} (z)	0.2 (z)	0.1 (z)	6×10^{-3} (z)
$\langle 3^3A'\|\mathcal{H}_{SO}\|2^1A'\rangle$	3×10^{-2} (z)	0.2 (z)	0.3 (z)	0.5 (z)
$\langle 1^3A''\|\mathcal{H}_{SO}\|X^1A'\rangle$	68.4 (x)/37.4 (y)	202.4 (x)/100.8 (y)	64.3 (x)/41.4 (y)	191.2 (x)/118.8 (y)
$\langle 1^3A''\|\mathcal{H}_{SO}\|2^1A'\rangle$	23.4 (x)/27.3 (y)	258.3 (x)/178.0 (y)	21.3 (x)/35.1 (y)	234.8 (x)/202.3 (y)
$\langle 1^3A''\|\mathcal{H}_{SO}\|3^1A'\rangle$	8.0 (x)/3.1 (y)	26.5 (x)/23.8 (y)	7.5 (x)/16.3 (y)	34.7 (x)/22.8 (y)
$\langle 1^3A'\|\mathcal{H}_{SO}\|1^1A''\rangle$	14.8 (x)/0.2 (y)	158.5 (x)/110.8 (y)	14.7 (x)/5.6 (y)	138.3 (x)/118.7 (y)
$\langle 2^3A'\|\mathcal{H}_{SO}\|1^1A''\rangle$	24.7 (x)/26.9 (y)	202.4 (x)/127.6 (y)	23.6 (x)/37.6 (y)	195.3 (x)/158.3 (y)
$\langle 3^3A'\|\mathcal{H}_{SO}\|1^1A''\rangle$	16.7 (x)/13.7 (y)	67.4 (x)/41.3 (y)	11.9 (x)/13.6 (y)	30.4 (x)/23.9 (y)
$\langle 1^3A''\|\mathcal{H}_{SO}\|1^1A''\rangle$	0.2 (z)	0.2 (z)	0.1 (z)	0.2 (z)
$\langle 2^3A''\|\mathcal{H}_{SO}\|X^1A'\rangle$	33.5 (x)/86.4 (y)	161.3 (x)/609.8 (y)	269.6 (x)/546.4 (y)	211.3 (x)/453.6 (y)

in the pyrone ring (X = O, Y = Se) strongly increases the SOMEs between the lowest-lying $n \rightarrow \pi^*$ type singlet (triplet) state and $\pi \rightarrow \pi^*$ type triplet (singlet) states in many, but not all of the tabulated cases. For example, the matrix element $\langle 1^3A''(n \rightarrow \pi^*)|\mathcal{H}_{SO,x}|2^1A'(\pi \rightarrow \pi^*)\rangle$ amounts to 277.1 cm^{-1} in PSO(O–Se) which corresponds to an increase of almost a factor of 30 compared to the parent psoralen. As the electronic coupling matrix element enters quadratically into the Golden Rule formula for radiationless transition rates, an increase by a factor of 1000 of the $S \rightsquigarrow T$ ISC rate for PSO(O–Se) compared to the parent psoralen seems plausible. The matrix element $\langle 1^3A''(n \rightarrow \pi^*)|\mathcal{H}_{SO,x}|3^1A'(\pi \rightarrow \pi^*)\rangle$ is less influenced and shows a lowering down to 2.9 cm^{-1} for PSO(O–Se) from a value of 10.8 cm^{-1} for the parent psoralen. On the contrary, selenium substitution solely in the 1-position at the furan side (X = Se, Y = O) does not bring about any appreciable changes for those tabulated SOMEs which involve the lowest lying singlet (S_3, $1^1A''$) or triplet (T_6, $2^3A''$) state of $n \rightarrow \pi^*$ type. Instead, for PSO(Se–-O) large SOMEs occur between the lowest triplet state of $\pi \rightarrow \sigma^*$ type (T_4, $1^3A''$) and some $\pi \rightarrow \pi^*$ excited singlet states. A hugh matrix element of 565.3 cm^{-1} for $\mathcal{H}_{SO,y}$ is also observed between T_4 and the ground state S_0.

These findings are intimately related to the $1/r^3$-dependence of the spin–orbit Hamiltonian: considerable spin–orbit integrals between two MOs will only arise if these MOs are located in the same spatial region. As the mean-field

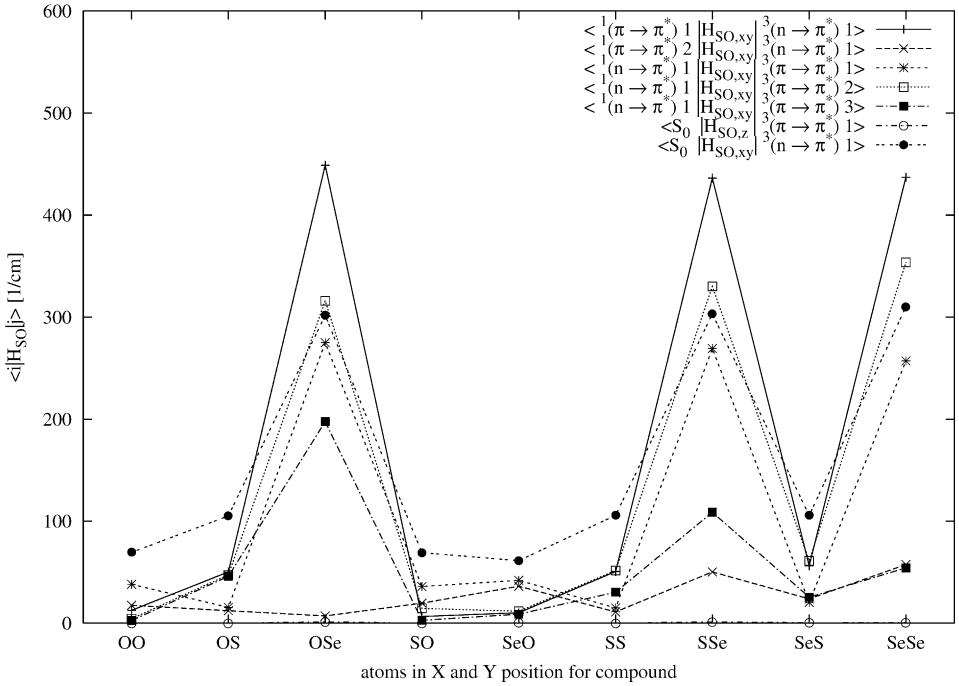

Fig. 4. Absolute values of spin–orbit matrix elements [cm^{-1}]. (Abscissa encoding corresponding to Fig. 1. If there is more than one nonvanishing Cartesian component of the spin–orbit Hamiltonian between to states the sum of their absolute values is depicted.)

operator is an (effective) one-electron operator, non-zero matrix elements occur only between configurations that are singly excited with respect to one another.

SOMEs will thus be significantly increased upon selenium substitution only if the above conditions are fulfilled for the main configurations of the states involved. For example, the (highest occupied) n orbital is localized at the carbonyl group for all heteropsoralens just as the MO n_{H-3} in Fig. 2. If the π orbital involved in the $\pi \rightarrow \pi^*$ excitation shows a noticeable amplitude in this region, the SOME between the lowest $n \rightarrow \pi^*$ excited states and this $\pi \rightarrow \pi^*$ excited state is expected be very large, e.g. in PSO(O–Se). Similarly, the large SOME $\langle 1^3A''(\pi \rightarrow \sigma^*)|\mathcal{H}_{SO,y}|1^1A'(S_0)\rangle$ in PSO(Se–O) can be explained by the amplitudes of the π and σ^* MOs at the 1-position in the furan ring.

Assuming that the shape and energetic order of the MOs and the electronic structure of the excited states are comparable for all the psoralens, a pronounced regularity in the size of the SOMEs is predicted. According to Fig. 4, this actually is the case to a large extent. One has to keep in mind, however, that these SOMEs are calculated at the respective ground state equilibrium geometry. Hetero-atom substitution may result in major changes in the adiabatic order of states. Hence, a similar regularity with respect to the time constants of spin-forbidden processes is by no means certain.

As discussed above, the $n \rightarrow \pi^*$ states are thought to be involved in the singlet–triplet ISC because of their appreciable SOMEs. At first sight, one might conclude that the ISC rate and as a consequence the triplet formation quantum yield will drop down sharply when the solvent polarity exceeds a certain value and the ISC channels involving the $n \rightarrow \pi^*$ states are not energetically accessible any more. Note, however, that Lim and others observed experimentally an increase of both the fluorescence and the triplet formation quantum yield upon increasing the solvent polarity or proticity. Of course, the quantum yield of triplet formation is a result of the competition of several processes. Among them, the internal conversion to the ground state plays a prominent role.

4. Conclusion

In this work, we have given a compilation of vertical electronic spectra and—for the first time—spin–orbit coupling matrix elements for psoralen and its sulfur and selenium substituted derivatives.

Our calculated absorption spectra are in close agreement with experimental values and previous TD-DFT calculations from the literature. Regarding the dependence of the energy of a specific state on the hetero-atom substitution pattern, our quantum chemical calculations are able to provide information about dark states which is difficult to access experimentally. More specific, the energy differences between low-lying excited states which are of great importance with respect to singlet–triplet ISC are found to vary strongly in the systems under study. The $n \rightarrow \pi^*$ states are lowered in energy by a large amount, when sulfur or selenium is present in the pyrone ring. The lowering of the $\pi \rightarrow \pi^*$ state S_1 is less pronounced. As a result, the $n \rightarrow \pi^*$ states become nearly degenerate to S_1 in our calculated vertical spectra for PSO(O–S) and PSO(O–Se). On the other hand, substitution inside the furan ring does almost not affect the energy of the $n \rightarrow \pi^*$ excited states, but lowers slightly the $\pi \rightarrow \pi^*$ state S_1 in energy. The energy gap between S_1 and the $n \rightarrow \pi^*$ excited states is thus increased for PSO(S–O) and PSO(Se–O). In the MO picture, these findings may be related to the strong localization of the n orbital near the carbonyl group. Similarly, the view of the $\pi \rightarrow \pi^*$ T_1 state as a diradical in the 5, 6 positions of the pyrone ring may explain that the energy of this state is almost constant for all psoralens under study.

In all heteropsoralens, low-lying $\pi \rightarrow \sigma^*$ excitations are found. We expect these states to be closely related to photochemical reactions involving bond cleavage and to the photostability of the psoralens.

In connection with the excitation energies, the calculated SOMEs allow to sketch the most important triplet state population mechanisms. For most of the systems, there are at least three triplet states of $\pi \rightarrow \pi^*$ and one of $n \rightarrow \pi^*$ character below or nearly degenerate to the S_1 state. Although the adiabatic excitation energies are unknown yet, we regard these states to be potentially involved in ISC processes starting from the adiabatically lowest excited singlet state. The latter may be of $\pi^* \rightarrow \pi^*$ or $n \rightarrow \pi^*$ type depending on the system and—probably—even the solvent. As all the coupling matrix elements between a singlet and a triplet $\pi \rightarrow \pi^*$ state in this energy regime are negligibly small, it is very likely that $^1(n \rightarrow \pi^*) \rightsquigarrow {}^3(\pi \rightarrow \pi^*)$ or $^1(\pi \rightarrow \pi^*) \rightsquigarrow {}^3(n \rightarrow \pi^*)$ are the dominant channels of ISC into the triplet state manifold. Note, however, that all $n \rightarrow \pi^*$ excited states exhibit a considerable blue shift in polar solvents and thus may not be accessible energetically. At first sight these findings contradict the experimental observation that the triplet quantum yield increases with increasing solvent polarity.

To resolve open questions which are connected with radiationless transitions in psoralens, a more detailed knowledge about the excited states in psoralens should thus be helpful. In a forthcoming publication we will discuss excited state equilibrium geometries, vibrational frequencies, and Franck–Condon factors for radiationless transitions. At the same time we will investigate the $\pi \rightarrow \sigma^*$ states in more detail.

Acknowledgements

Funding by the Deutsche Forschungsgemeinschaft (DFG) through project Ma 1051/5-1 is gratefully acknowledged. It is a pleasure to thank Stefan Grimme (Münster) and Mirko Waletzke for making their DFT/MRCI code available to us.

References

[1] D. Averbeck, Photochem. Photobiol. 50 (1989) 859–882.
[2] W.M. Horspool, P.-S. Song (Eds.), CRC Handbook of Organic Photochemistry and Photobiology, CRC Press, Boca Raton, FL, 1995.
[3] F. Dall'Aqua, D. Vedaldi, in: W.M. Horspool, P.-S. Song (Eds.), CRC Handbook of Organic Photochemistry and Photobiology, CRC Press, Boca Raton, FL, 1995, pp. 1357–1366.
[4] G.G. Aloisi, F. Elisei, S. Moro, G. Miolo, F. Dall'Acqua, Photochem. Photobiol. 71 (2000) 506–513.
[5] P.-S. Song, J.K.J. Tapley, Photochem. Photobiol. 29 (1979) 1177–1197.
[6] Shim, in: W.M. Horspool, P.-S. Song (Eds.), CRC Handbook of Organic Photochemistry and Photobiology, CRC Press, Boca Raton, FL, 1995, pp. 1347–1356.
[7] A. Harriman, in: W.M. Horspool, P.-S. Song (Eds.), CRC Handbook of Organic Photochemistry and Photobiology, CRC Press, Boca Raton, FL, 1995, pp. 1374–1378.
[8] J. Llano, J. Raber, L.A. Eriksson, J. Photochem. Photobiol. A: Chem. 154 (2003) 235–243.
[9] G. Mugesh, W.-W. du Mont, H. Sies, Chem. Rev. 101 (2001) 2125–2179.
[10] S.R. Rajski, R.M. Williams, Chem. Rev. 98 (1998) 2723–2796.
[11] M. Collet, M. Hoebeke, J. Piette, A. Jakobs, L. Lindqvist, A.V. de Vorst, J. Photochem. Photobiol. B: Biol. 35 (1996) 221–231.
[12] M. Collet, E. Sage, J. Piette, Photochem. Photobiol. 66 (1997) 214–223.
[13] R.V. Bensasson, E.J. Land, C. Salet, Photochem. Photobiol. 27 (1978) 273–280.
[14] T. Wolff, H. Görner, Phys. Chem. Chem. Phys. 6 (2004) 368–376.
[15] W.W. Mantulin, P.-S. Song, J. Am. Chem. Soc. 95 (1973) 5122–5129.
[16] P.-S. Song, M.L. Harter, T.A. Moore, W.C. Herndon, Photochem. Photobiol. 14 (1971) 521–530.
[17] T. Lai, B.T. Lim, E.C. Lim, J. Am. Chem. Soc. 104 (1982) 7631–7635.
[18] E.C. Lim, J. Phys. Chem. 90 (1986) 6770–6777.
[19] A. Nakata, T. Baba, H. Takahashi, H. Nakai, J. Comput. Chem. 25 (2004) 179–188.
[20] S. Grimme, M. Waletzke, J. Chem. Phys. 111 (1999) 5645–5655.
[21] M. Kleinschmidt, J. Tatchen, C.M. Marian, J. Comp. Chem. 23 (2002) 824–833.
[22] A. Schäfer, C. Huber, R. Ahlrichs, J. Chem. Phys. 100 (1994) 5829.
[23] R. Ahlrichs, M. Bär, H.-P. Baron, R. Bauernschmitt, S. Böcker, P. Deglmann, M. Ehrig, K.E. Chkorn, S. Elliott, F. Furche, F. Haase, M. Häser, C. Hättig, H. Horn, C. Huber, U. Huniar, M. Kattannek, A. Köhn, C. Kölmel, M. Kollwitz, K. May, C. Ochsenfeld, H. Öhm, A. Schäfer, U. Schneider, M. Sierka, O.T. Eutler, B. Unterreiner, M. von Arnim, F. Weigend, P. Weis, H. Weiss, Turbomole (vers. 5.6), Universität Karlsruhe, 2002.
[24] A.D. Becke, J. Chem. Phys. 98 (1993) 5648–5652.
[25] P.J. Stephens, F.J. Devlin, C.F. Chabalowski, M.J. Frisch, J. Phys. Chem. 98 (1994) 11623–11627.
[26] A.D. Becke, J. Chem. Phys. 98 (1993) 1372–1377.
[27] C. Lee, W. Yang, R.G. Parr, Phys. Rev. B 37 (1988) 785.
[28] M. Kleinschmidt, C.M. Marian, Chem. Phys., 2004, accepted for publication.
[29] B.A. Heß, C.M. Marian, U. Wahlgren, O. Gropen, Chem. Phys. Lett. 251 (1996) 365–371.
[30] J. Tatchen, C.M. Marian, Chem. Phys. Lett. 313 (1999) 351–357.
[31] A. Klamt, G. Schüürmann, J. Chem. Soc., Perkin Trans. 2 (1993) 799.
[32] A. Schäfer, A. Klamt, D. Sattel, J.C.W. Lohrenz, F. Eckert, Phys. Chem. Chem. Phys. 2 (2000) 2187–2193.
[33] R.C. Weast (Ed.), CRC Handbook of Chemistry and Physics, 66th ed., CRC Press, Boca Raton, FL, pp. 1985–1986.
[34] H. Matsumoto, Y. Ohkura, Chem. Pharm. Bull. 26 (1978) 3433–3439.
[35] M. Klessinger, J. Michl, Excited States and Photochemistry of Organic Molecules, VCH Publishers, Inc., Weinheim, Germany, 1995.
[36] C. Marian, in: K. Lipkowitz, D. Boyd (Eds.), Reviews in Computational Chemistry, vol. 17, Wiley-VCH, Weinheim, 2001, pp. 99–204.